A multibeam opportunistic SAR system

Edison Cristofani, Virginie Kubica, Xavier Neyt
Electrical Engineering Dept., Royal Military Academy, Belgium
Edison.Cristofani@elec.rma.ac.be

***Abstract*—This paper discusses the implementation of a passive radar system designed to perform imaging of the ground using radar satellites as emitters of opportunity. The receiver consists in a 4-element microstrip antenna array and is able to receive the signals from most C-band Synthetic Aperture Radar satellites. The array antenna is used to attenuate the direct-path signal by null-steering.**

The successive processing steps are described with focus on the signal synchronization, signal separation and the image formation algorithm. The current results are presented and discussed.

I. Introduction

SAR imaging has been historically performed using monostatic radar configurations where the transmitter and receiver shared the same location. Reconstructed target images are obtained after processing several received echoes of a same scatterer from different azimuth angles, taking advantage of the displacement of the radar system to synthesize a large aperture.

Bistatic SAR imaging is certainly not new. Cooperative bistatic SAR has been conducted either air-air [1], air-space [2], [3] and also space-space [4], [5] with the TanDEM-X mission. Ground-based bistatic SAR imaging with spaceborne illuminators of opportunity is also described in [6], [7]. The main challenge reported is the synchronization between the transmitter and the receiver in opportunistic systems. This problem is typically resolved by acquiring separately the signal received directly from the satellite (direct-path signal or reference signal) using a dedicated antenna. In the system that will be presented in this paper the reference signal is extracted from the scattered signals without a dedicated antenna. It should also be noted that since the transmitter of opportunity is a radar system designed to perform imaging, the transmitted signal will always be suitable for bistatic imaging. Suitability of an opportunistic signal for radar application can be assessed using the ambiguity function. The presence of large ambiguities and more generally of large sidelobes in the ambiguity function denote a waveform that will lead to ghosts in the produced image.

Bistatic SAR imaging presents several interesting advantages. The system is relatively cheap as transmitters of opportunity are used. Since different transmitters of opportunity can be used, a higher combined revisit time can be achieved than using a single satellite. And last but not least, from a tactical point of view, these systems are difficult to detect and easy to deploy due to their small size. Bistatic opportunistic SAR systems are however subject to the actual availability of a transmitter of opportunity. In addition, when a ground-based receiving system is considered, and depending on the application and the exact configuration of the scenario, the viewing geometry is not favorable since the receiving incidence angle is typically very small.

This paper describes a low-cost passive radar system operating in C band. The system uses illuminators of opportunity in a bistatic radar configuration to produce SAR images of the ground.

The receiver is tailored to moving space-borne C-band illuminators of opportunity such as the SAR instruments carried by Envisat, ERS-2, RADARSAT and RADARSAT-2. These instruments transmit linearly frequency modulated chirps with a minimum bandwidth of 11 MHz. When combined, these satellites present a very attractive revisit time, providing with as much as 42 passes a month for a same latitude, including ascending and descending passes.

A description of the reception chain of the designed passive radar system, the viewing geometry and the acquisition system is given in Section II. Data processing steps such as signal separation, signal synchronization, signal parameters extraction and SAR imaging formation are described in Section III. Results obtained from actual data are presented and discussed in Section IV. Finally, Section V concludes the paper.

II. System description

A block diagram of the receiving system, showing both the hardware and software stages, is depicted in Fig. 1.

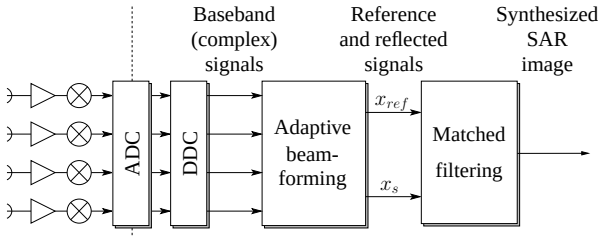

Fig. 1. Block diagram of the entire passive radar system.

The radio frequency (RF) signal transmitted by an illuminator of opportunity is first received, amplified and down-converted to intermediate frequencies (IF). The IF signal is then sampled and further numerically down-converted to base band, resulting in a dataset of four phase-shifted versions of the received signal. In the next block, adaptive beamforming is performed to separate the reference signal (direct-path signal) and the reflected signal. In the final block, an image is

synthesized from the separated signals acquired during an overpass of a SAR satellite. These blocks are described in more detail in the next sections.

A. Reception system

The implemented system includes a uniform linear array (ULA) of four vertically polarized microstrip antennas with a center-to-center separation of $\lambda/2$. The calibration of this array is discussed in a companion paper [8]. Each antenna has a gain of 7.5 dBi and is designed to operate at a resonance frequency of approximately 5.4 GHz presenting a bandwidth wide enough to cover the four SAR instruments that will be used as illuminators of opportunity, as described in Table I.

Satellite	Center frequency	Bandwidth
Envisat	5.331 GHz	16 MHz
ERS-2	5.300 GHz	16 MHz
RADARSAT	5.300 GHz	11.6 up to 30 MHz
RADARSAT 2	5.405 GHz	11.6 up to 100 MHz

TABLE I
SATELLITE SAR INSTRUMENT CHARACTERISTICS.

The receiving system (see Fig. 2) is a typical superheterodyne receiver with three main stages: RF reception and amplification, down-conversion to IF and sampling.

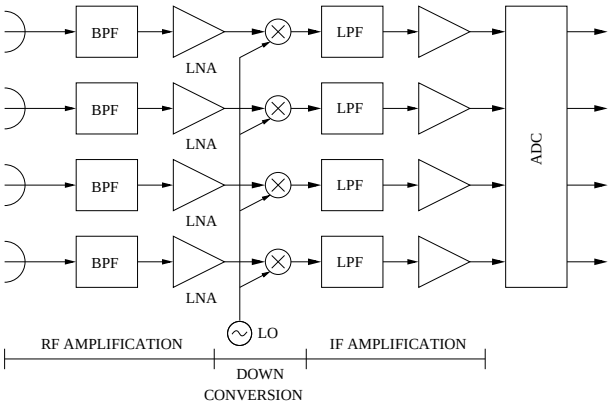

Fig. 2. Block diagram of the implemented multichannel receiver.

In the amplification stage, signals are received and amplified using a cascade of low noise amplifiers summing up a total amplification gain of 75 dB. The local oscillator (LO) used in the down-conversion is programmable in order to be able to fit the signal of the different satellites in the bandwidth of the A/D card. The IF signal is then, after a 25 dB amplification, sampled at 50 MSamples/s using a 16-bit A/D card (AlazarTech ATS660) and digitally down-converted to base band in the third stage.

B. Viewing geometry and range resolution

The considered satellites are on LEO near-polar orbits. This means they fly roughly from north to south or from south to north. The radar instruments on-board the considered satellites are side-looking (roughly east-wards or west-wards). The reception system has a relatively wide azimuth opening angle and is pointed East.

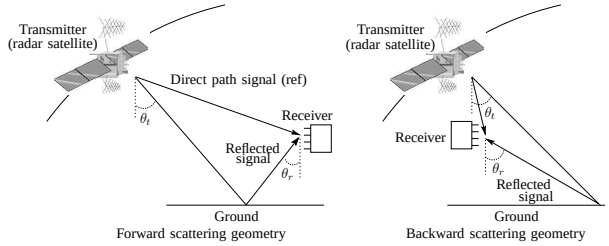

Fig. 3. Possible imaging scenarios. Left: back scattering geometry, both illuminator and receiving system are on the same side. Right: forward scattering geometry, target is between illuminator and receiver.

Hence if the satellite is right looking (e.g. ERS-2, Envisat, RADARSAT), ascending passes will yield a backward scattering geometry while descending passes will yield a forward scattering geometry. Ground range resolution in a flat reflection area can be approximated by [6]

$$\Delta r_g = \frac{c}{B|\sin(\theta_t) + \sin(\theta_r)|} \tag{1}$$

where c stands for the speed of light in free space, B is the bandwidth of the chirp and θ_t and θ_r are the incident angles with respect to the ground plane for the transmitter and receiver, respectively. And hence the backward scattering scenario is more favorable than the forward scattering scenario as far as range resolution is considered. On the other hand, the scattered signal amplitude is typically higher in forward scattering scenarios [9].

In the considered forward scattering geometry scenario these parameters would be $\theta_t \simeq 20°$ and $\theta_r \simeq -75°$ since the receiving antennas are oriented $15°$ below the horizon, yielding $\Delta r_g \simeq 30$ m. In the considered backward scattering geometry, the incident angle of the receiver would be modified to $\theta_r \simeq 75°$, providing a ground range resolution of about 14 m.

C. Signal acquisition

Overpass times of the satellites are predicted using the SGP4 orbit propagator, taking into account the satellite's antenna footprint. The Two-Line Elements (TLE) used as input to the orbit propagator are regularly updated in order to minimize prediction error. Due to the limited accuracy of the prediction, the start of the data acquisition needs to be triggered. The trigger is based on the amplitude of the received signals. Very much like in CFAR (Constant False Alarm Rate) systems, the variance of the ambient noise and interference is "learned" and serves to adjust the triggering threshold. Acquisition at 50MS/s leads to a data rate of 400MB/s for a 4-channel receiving system.

III. DATA PROCESSING

A. Signal separation

The direct-path signal and the reflected signals have to be separated from one another. If used to correlate with the echo-

signal, the direct-path signal has to be free of echo signal, hence the need for separation. In the present case, the direct-path signal can be reconstructed since its general shape is known (it is a linear FM chirp). The only unknown is the initial phase that can be estimated from the direct-path signal. Due to the large amplitude of the direct-path signal, this estimation is not impacted by the presence of echo signal. Separation also serves to attenuate the range sidelobes in the image due to the direct-path signal.

In future works, signal separation will be achieved by using the array of the receiver to steer a null in the direction of the satellite. As a linear array is considered, this of course produces a shadow on the ground.

B. Signal synchronization

A major issue in space-to-ground, non-collaborative radar systems as the one presented in this paper is the lack of phase synchronization between transmitters and the receiver.

The n-th transmitted chirp from an illuminator can be expressed as

$$s_{tx,n} = e^{j(\phi_{0,n}+2\pi f_0 t+\frac{\alpha}{2}t^2)} \tag{2}$$

where f_0 and $\phi_{0,n}$ are the center frequency and unknown phase of n-th chirp at the transmitter's local oscillator respectively, and α is the chirp rate. The signal is received with a time delay Δt_n. This time delay adds an additional quadratic phase term to the received signal and is responsible for the characteristic quadratic phase evolution along the synthetic aperture.

After down-conversion, i.e., multiplying with the local oscillator signal $e^{-j(\phi_{1,n}+2\pi f_1 t)}$, where f_1 and $\phi_{1,n}$ are respectively the center frequency and unknown phase of the receiver's local oscillator, one obtains

$$\begin{aligned} s_{rx,n} &= e^{j[(2\pi(f_0-f_1)+\alpha\Delta t_n)t+\frac{\alpha}{2}t^2]} \\ &\quad e^{j[\phi_{0,n}-\phi_{1,n}-2\pi f_0\Delta t_n+\frac{\alpha}{2}\Delta t_n^2]} \end{aligned} \tag{3}$$

The constant phase component

$$\phi_{0,n} - \phi_{1,n} - 2\pi f_0 \Delta t_n + \frac{\alpha}{2}\Delta t_n^2 \tag{4}$$

and the residual frequency term $2\pi(f_0 - f_1) + \alpha\Delta t_n$ are estimated from the direct path signal. The term depending on Δt_n can be subtracted as Δt_n is proportional to the distance between the satellite and the receiver when the n-th chirp was transmitted, yielding the unknown phase term $\phi_{0,n} - \phi_{1,n}$.

C. Parameters extraction

An estimate of the constant phase term (4) is obtained as follows. The direct-path chirp is easily located due to its high amplitude. The phase of the received signal is unwrapped and fitted using the phase of (3) yielding an estimate for the constant phase term, for the frequency term and for α. This procedure is illustrated in Fig. 4, showing the characteristic quadratic phase of a linear FM chirp after unwarping of the phase.

A reference chirp is reconstructed from the extracted parameters. Fig. 5 shows that the matching between the theoretical and the measured signals is relatively accurate.

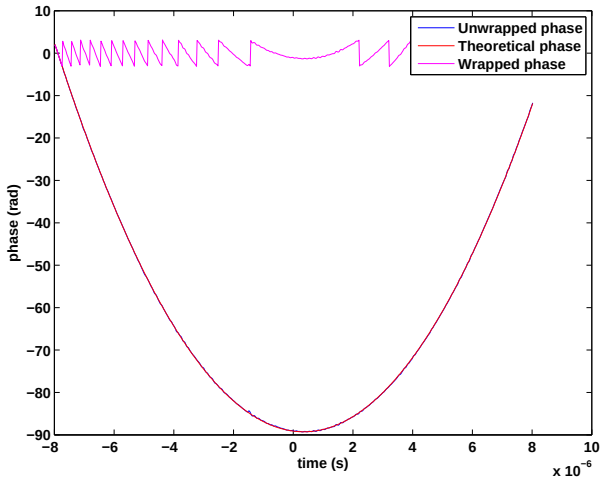

Fig. 4. Unwrapped phase history of one of the received ERS-2 chirps. Although some artifacts are present in the measured wrapped phase, the unwrapped and the theoretical phase present a similar evolution.

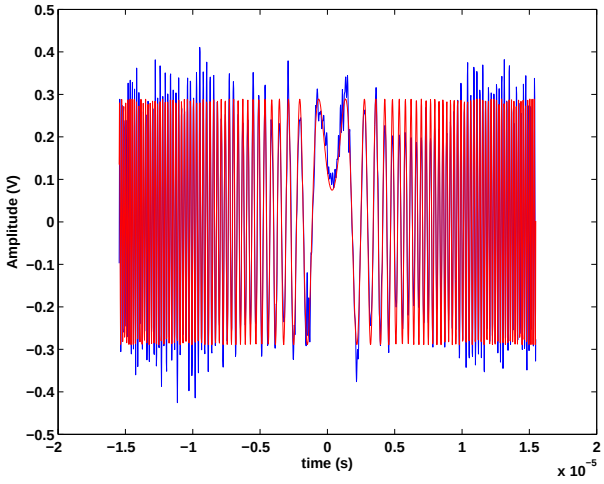

Fig. 5. Comparison between the actual chirp (blue) and the synthesized chirp based on the estimated parameters.

This same process is repeated for each received chirp, providing estimates of the unknown phase term $\phi_{0,n} - \phi_{1,n}$ at each pulse.

D. Image formation algorithm

Since the receiver is non-moving, the expression of the azimuth phase history is much more simple than that of the general bistatic case. And although the authors are well aware of Loffeld's bistatic formula [10] and derived works leading to FFT-based processors [11], another path is followed as the areas where a useful image is obtained are much smaller than the satellite's footprint. The image synthesis is based on the direct application of the matched filter. As this would be extremely time consuming, the processing is, after the usual range-compression step, approached by integrating the raw data along the azimuth locus (bistatic range as a function of the azimuth position of the transmitter) of the considered scatterer, taking into account the azimuth phase history [12].

The azimuth locus is computed for each image pixel in ground range. The added benefit is that the image is directly obtained in ground range and no separate geocoding step needs to be performed.

IV. Results

A. Data acquisition

The receiving system was placed on the roof of a building overlooking an urban area in Brussels, Belgium and an optical image of the viewing area is presented in Fig. 6.

Fig. 6. Optical image of the viewing area as seen from the receiving system.

The real part of a signal acquired during an overpass of the Envisat satellite is presented in Fig. 7. Chirps transmitted by Envisat are grouped into 30-ms bursts and with remarkable variations in amplitude and pulse repetition frequency (PRF) between groups. These variations correspond to the different beams produced by the electronic antenna of this satellite when scanning the swath in wide-swath mode.

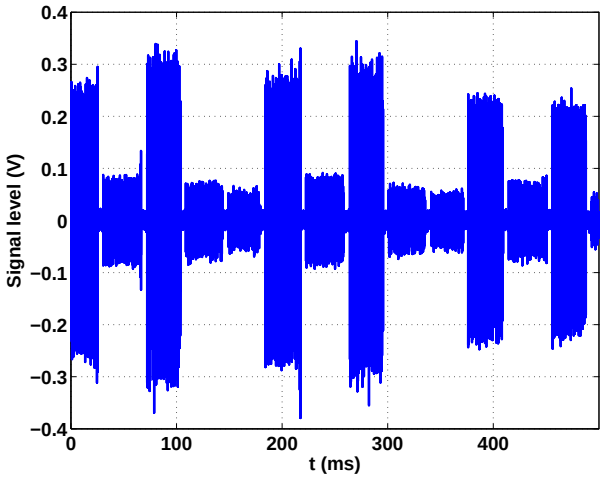

Fig. 7. Real part of the signal acquired during an overpass of the Envisat satellite.

B. Range compression

The acquired data stream is divided into chunks corresponding to a single chirp and its echoes. The location of the direct-path chirp is obtained by correlation with a synthetic chirp. The estimate of the unknown phase is taken into account in the range compression hence removing that unknown phase component. A range-compressed image of an ERS-2 acquisition is depicted in Fig. 8 showing the large correlation peaks of the reference signal and, further away in range, possible echoes from scatterers.

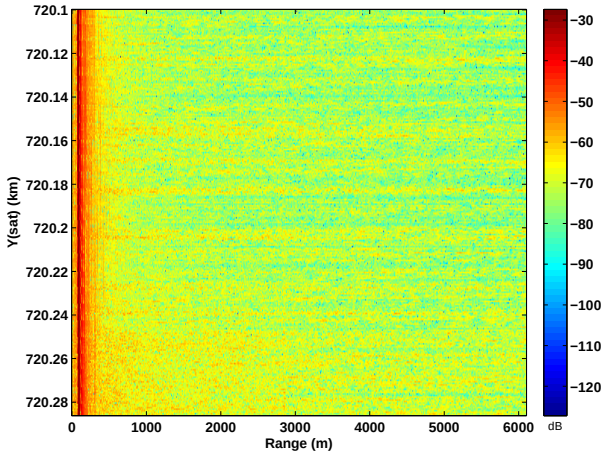

Fig. 8. Range-compressed image of an ERS-2 acquisition using a synthesized reference signal.

C. Azimuth compression

Figure 9 is obtained by performing the range and azimuth compression at regularly-spaced range intervals using two different range-windows. The use of range-windows aims at reducing the range sidelobes that may obscure reflections from the imaged area. When a rectangular range window is used,

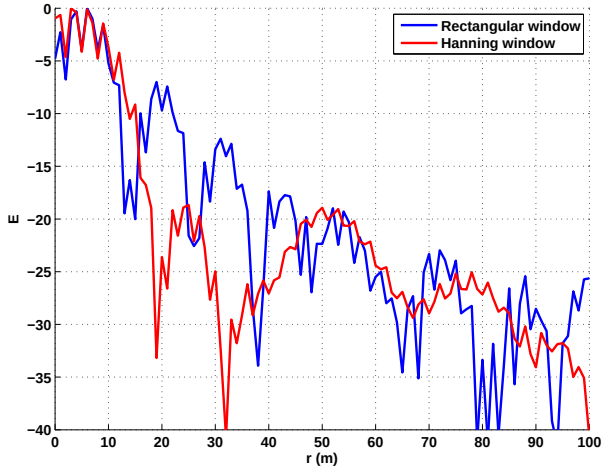

Fig. 9. Comparison of a scan in range using rectangular and Hanning windowing.

the first null is located at 14m. When a Hanning window is

used, the first null is located at 19m, indeed leading to a loss in resolution as is well known.

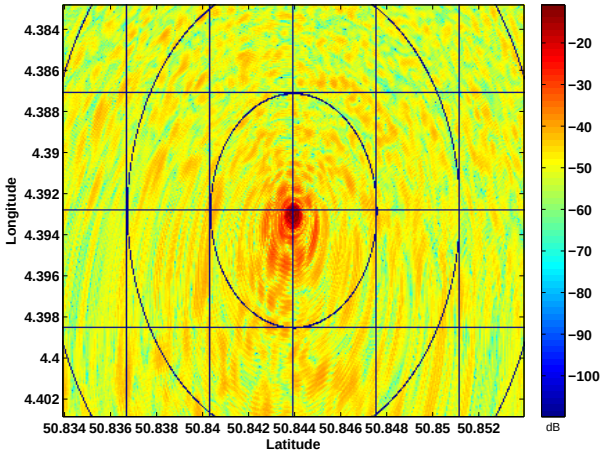

Fig. 10. Bistatic SAR image using ERS-2 signal. The receiver is located at the center of the figure.

Figure 10 presents a single-look azimuth-compressed SAR image, the amplitude is logarithmically scaled (dB). The image is centered at the receiver. Isodistance rings are spaced 400m apart from the receiver while the distance of the lines of the grid is 400m as well. Obviously, the largest signal is located at the receiver's position, and side lobes appear, although attenuated due to the use of a Hanning range window (no azimut-windowing is used).

Figure 11 shows the single-look azimuth-compressed SAR image of the receiver's field of view. The radiation diagram of the receiving antenna points roughly East (down on the image). It is not obvious to relate what is seen in these images to the optical image of Fig. 6. The presence of actual signal is assessed in the next section. A more meaningful image might be obtained by placing the receiver such that it actually overlooks a wide area.

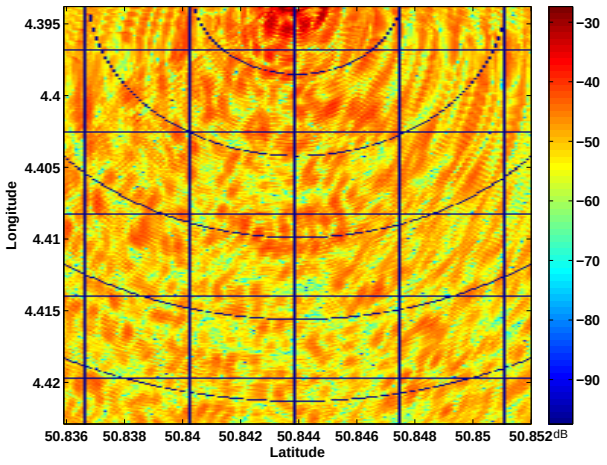

Fig. 11. SAR image centered on the viewing area of the system.

D. Assessment of the received data

To assess the presence of non-noise data, the distribution (observed frequency) of the scattering coefficients in the imaged area were compared. Figure 12 presents the distribution of the amplitude of the scattering coefficients in two distinct areas. The first area is located directly under the main beam of the antenna of the receiving system. In this area, echo and noise signal is expected. The second area is located on the left of the antenna, where the gain of the receiving antenna is minimal. In that area, only noise (and interferences) is expected. As can be seen, the distribution of the scattering

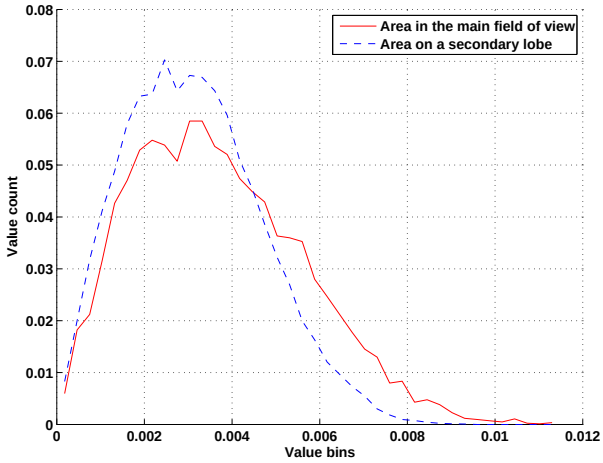

Fig. 12. Distributions (frequency) of the amplitude of the scattering coefficients over two areas in the obtained SAR image. In green, an area located in the main field of view of the receiving antenna. In red, an area in a secondary lobe.

coefficients in the receiving antenna footprint is indeed slightly shifted to the higher values when compared to the distribution of the scattering coefficients on the side of the antenna. This indicates that there is indeed a contribution from echo signals and that what is seen is not exclusively noise.

V. Conclusions and Future Work

This paper presents a passive radar system for SAR imaging using imaging radar satellites as transmitter of opportunity. The challenges arising when using transmitters of opportunity were discussed. Phase synchronization is obtained by recording the phase of the direct-path chirp and image synthesis is performed by matched filtering. Azimuth compression is performed by integrating along the hyperbola in the (range,azimuth) plane.

First results were presented. The imaging geometry, and in particular the fact that the receiver is looking at an extremely dense scene under grazing incidence complicates the interpretation of the resulting image.

Besides the relocation of the receiver, further work include the comparison of the resulting image with classical monostatic SAR images to assess the differences.

REFERENCES

[1] P. Dubois-Fernandez, H. Cantalloube, B. Vaizan, G. Krieger, R. Horn, M. Wendler, and V. Giroux, "ONERA-DLR bistatic SAR campaign: planning, data acquistiton, and first analysis of bistatic scattering behaviour of natural and urban targets," *IEEE Proceedings – Radar, Sonar and Navigation*, vol. 153, pp. 214–223, June 2006.

[2] M. Rodriguez-Cassola, S. Baumgartner, G. Krieger, and A. Moreira, "Bistatic TerraSAR-X/F-SAR spaceborne-airborne SAR experiment: Description, data processing, and results," *IEEE Trans. on Geoscience and Remote Sensing*, vol. 48, pp. 781–794, Feb. 2010.

[3] I. Walterscheid, T. Espeter, A. Brenner, J. Klare, J. Ender, H. Nies, R. Wang, and O. Loffeld, "Bistatic SAR experiments with PAMIR and TerraSAR-X setup, processing, and image results," *IEEE Trans. on Geoscience and Remote Sensing*, vol. 48, pp. 3268 – 3279, Aug. 2010.

[4] G. Krieger, I. Hajnsek, K. Papathanassiou, M. Younis, and A. Moreira, "Interferometric synthetic aperture radar (SAR) missions employing formation flying," *Proceedings of the IEEE*, vol. 98, pp. 816–843, May 2010.

[5] M. Eineder, G. Krieger, and A. Roth, "First data acquisition and processing concepts for the TanDEM-X mission," in *Proceedings of ISPRS (International Society for Photogrammetry and Remote Sensing) Commission I Symposium*, (Paris, France), 2006.

[6] J. Sanz-Marcos, P. Lopez-Dekker, J. J. Mallorqui, A. Aguasca, and P. Prats, "SABRINA: A SAR bistatic receiver for interferometric applications," *IEEE Geoscience and Remote Sensing Letters*, vol. 4, Apr. 2007.

[7] A. Broquetas, P. Lopez-Dekker, J. J. Mallorqui, A. Aguasca, M. Fortes, J. C. Merlano, and S. Duque, "SABRINA-X: Bistatic SAR receiver for TerraSAR-X," in *8th European Conference on Synthetic Aperture Radar*, (Aachen, Germany), 2010.

[8] V. Kubica, R. Hock, E. Cristofani, and X. Neyt, "Strategies for the calibration of an array of patch antennas in passive bistatic SAR imaging," in *Proc. of the IEEE Radar conference*, (Kansas City, MI), May 2011.

[9] N. J. Willis and H. D. Griffiths, *Advances in Bistatic Radar*. Raleigh, NC: SciTech Publishing, 2007.

[10] O. Loffeld, H. Nies, V. Peters, and S. Knedlik, "Models and useful relations for bistatic SAR processing," in *Proc. of the IEEE Int. Geoscience and Remote Sensing Symposium*, vol. 3, pp. 1442–1445, July 2003.

[11] K. Natroshvili, O. Loffeld, H. Nies, and A. Ortiz, "First steps to bistatic focusing," in *Proc. of the IEEE Int. Geoscience and Remote Sensing Symposium*, vol. 2, pp. 1072–1076, July 2005.

[12] D. D'Aria, A. Guarnieri, and F. Rocca, "Focusing bistatic synthetic aperture radar using dip move out," *IEEE Trans. on Geoscience and Remote Sensing*, vol. 42, pp. 1362–1376, July 2004.